Dynamics in the anisotropic *XY* model driven by dichotomous Markov noise

Katsuya Ouchi,[1,*] Takehiko Horita,[2,†] Naofumi Tsukamoto,[3] Naoya Fujiwara,[3] and Hirokazu Fujisaka[3]
[1]*Kobe Design University, 8-1-1 Gakuennishi-Machi, Nishi-ku, Kobe 651-2196, Japan*
[2]*Department of Mathematical Sciences, Osaka Prefecture University, 1-1 Gakuencho, Sakai 599-8531, Japan*
[3]*Department of Applied Analysis and Complex Dynamical Systems, Graduate School of Informatics, Kyoto University, Kyoto 606-8501, Japan*
(Received 30 May 2008; published 28 August 2008)

The statistics of a subcritical spatially homogeneous *XY* spin system driven by dichotomous Markov noise as an external field is investigated, particularly focusing on the switching process of the sign of the order parameter parallel to the external field. The switching process is classified in two types, which are called the Bloch-type switching and the Ising-type switching, according to whether or not the order parameter perpendicular to the external field takes finite value at the switching. The phase diagram for the onset of the switching process with respect to the amplitude of the external field and the anisotropy parameter of the system is constructed. It is revealed that the power spectral density $I(\omega)$ for the time series of the order parameter in the case of the Bloch-type switching is proportional to $\omega^{-3/2}$ in an intermediate region of ω. Furthermore, the scaling function of $I(\omega)$ near the onset point of the Bloch-type switching is derived.

DOI: 10.1103/PhysRevE.78.021139 PACS number(s): 02.50.−r, 05.40.−a, 64.60.Ht

I. INTRODUCTION

Over the last decade, the dynamics of the magnetization in ferromagnetic systems below the critical temperature driven by a periodically temporary oscillating external magnetic field has been extensively studied [1–5]. After the first work in a deterministic mean-field system by Tome *et al.* [1], much progress has been made in terms of Monte Carlo simulations of a kinetic Ising spin system [2]. It was found that concerning the prescribed symmetry $F(t+\frac{T}{2})=-F(t)$ of the external field $F(t)$ the system shows two kinds of oscillations called symmetry-restoring oscillation and symmetry-breaking oscillation depending on the amplitude and frequency of the applied external field, and that the transition between the two oscillations belongs to the same universality class of the equilibrium Ising model in zero field. The transition is called the dynamic phase transition (DPT). With a constant bias of the external field, DPT was also shown to belong to the same universality class of the Ising model in nonzero field [3]. DPT has also been observed experimentally in an ultrathin Co film on Cu(100) [4].

Recently Fujisaka *et al.* proposed a simple mean-field model to investigate the origin of DPT in the Ising spin system [5]. Furthermore, they generalized the framework of DPT to the *XY* spin system in a periodically oscillating magnetic field by introducing the following equation of motion [6]:

$$\dot{\psi}(t) = \psi - |\psi|^2\psi + \gamma\psi^* + F(t) \tag{1}$$

and its spatially extended case [7], where ψ is the complex order parameter, γ is a real anisotropy parameter, and $F(t)=h\cos(\Omega t)$ is the applied external field satisfying $F(t+\frac{\pi}{\Omega})=-F(t)$.

It is quite interesting to ask whether DPT would be observed under other kinds of external fields, e.g., a temporally stochastic and spatially uniform field with finite amplitude. Ising spin systems driven by such an external field were investigated and DPT was observed [8,9]. We have studied DPT in a mean-field model of Ising system driven by such an external field of another kind, the symmetric dichotomous Markov noise (DMN) [10], where a large amount of studies on the behavior of systems driven by DMN exists as reviewed by Bena [11]. We also found that there exist two kinds of motions called symmetry-restoring motion (SRM) and symmetry-breaking motion (SBM) analogous to the symmetry-restoring oscillation and the symmetry-breaking oscillation in the periodically oscillating case [12]. The dynamics of a spatially distributed Ising spin system in the case of SBM was then studied focusing on the domain size statistics [13]. Here we will investigate the dynamics of the spatially homogeneous *XY* spin system driven by DMN in the context of DPT. The order parameter of the system obeys Eq. (1) with $F(t)$ being DMN instead of the periodically oscillating external field. The purpose of the present paper is to clarify the difference of the dynamics in the *XY* spin system from the one in the Ising spin system and to characterize the statistical properties, especially, of real component of $\psi(t)$ parallel to the external field.

This paper is organized as follows. The linear stability analysis of Eq. (1) in both cases of $F(t)$ being a constant and DMN is presented in Sec. II. The phase diagram for the onset of switching is shown, and the parameter region, where the asymptotic dynamics reduces to a Ising spin system, and a summary on the statistics are provided. The dynamics characteristic to the *XY* spin system is discussed in Sec. III. In Sec. IV, another type of dynamics characteristic to the *XY* spin system, which is a mixture of the dynamics appearing in the Ising spin system and that discussed in Sec. III is discussed. Concluding remarks are given in Sec. V.

*ouchi@kobe-du.ac.jp
†horita@ms.osakafu-u.ac.jp

II. LINEAR STABILITY ANALYSIS AND PHASE DIAGRAM

We examine the asymptotic dynamics of the complex order parameter $\psi(t)$ obeying Eq. (1), or equivalently its real and imaginary parts of $X(t)$, and $Y(t)$ obeying the equations of motion

$$\dot{X}(t) = -\frac{\partial V[X,Y;F(t)]}{\partial X} = (1+\gamma-Y^2)X - X^3 + F(t), \tag{2a}$$

$$\dot{Y}(t) = -\frac{\partial V[X,Y;F(t)]}{\partial Y} = (1-\gamma-X^2)Y - Y^3, \tag{2b}$$

with the potential $V(X,Y;F) \equiv \frac{1}{4}(X^2+Y^2-1)^2 - \frac{\gamma}{2}(X^2-Y^2) - FX$. Here $F(t)$ is the symmetric DMN which alternates between $+H_0$ and $-H_0$ with the transition rate τ_F^{-1}. The probability density $p(\tau)$ of the time interval τ for the transitions of $F(t)$ is given by

$$p(\tau) = \tau_F^{-1} e^{-\tau/\tau_F}. \tag{3}$$

The system of Eqs. (2) is invariant under the transformation $X \to -X$ and $F(t) \to -F(t)$. Since $F(t)$ also has statistical symmetry, i.e., $F(t)$ and $\tilde{F}(t) = -F(t)$ are statistically equivalent, the system has either symmetric asymptotic solution or a pair of asymptotic solutions symmetric with each other. We are now interested in the event that $X(t)$, parallel component of $\psi(t)$ to the external field $F(t)$, changes its sign, which is called the switching. The time interval between two successive switching events is then called the switching time. Since $\dot{Y}=0$ for $Y=0$, hereafter, the phase space is restricted to the upper half-plane $\{(X,Y) \mid Y \geqslant 0\}$.

A. Linear stability analysis under constant external field

Let us first consider the fixed points of Eqs. (2) by replacing $F(t)$ with the constant σH_0 with σ denoting plus or minus. By considering the minima of the potential $V(X,Y;\sigma H_0)$, one finds four kinds of stable fixed points depending on the parameter values of γ and H_0.

(i) If $\gamma > 0$ and $H_0 < 2\gamma\sqrt{1-\gamma}$: Two fixed points

$$[\sigma g(\theta_0), 0], \quad [\sigma g(\theta_0 + 2\pi/3), 0] \tag{4}$$

exist, where $g(\theta) \equiv \frac{2\sqrt{1+\gamma}}{\sqrt{3}} \cos\theta$, $\theta_0 \equiv \frac{1}{3}\cos^{-1}[-H_0/H_c(\gamma)]$, and

$$H_c(\gamma) \equiv 2\left(\frac{1+\gamma}{3}\right)^{3/2}. \tag{5}$$

Here $H_c(\gamma)$ gives the threshold value of H_0 between SRM and SBM [12] in the Ising-type equation of motion

$$\dot{X}_I(t) = (1+\gamma)X_I - X_I^3 + F(t), \tag{6}$$

to which Eq. (2a) reduces with $Y=0$.

(ii) If $H_0 > 2|\gamma|\sqrt{1-\gamma}$ and $H_0 < H_c(\gamma)$: One fixed point

$$[\sigma g(\theta_0 + 2\pi/3), 0] \tag{7}$$

exists. The fixed point $[\sigma g(\theta_0), 0]$ existing in the region (i) loses its stability in the Y direction at the boundary between (i) and (ii).

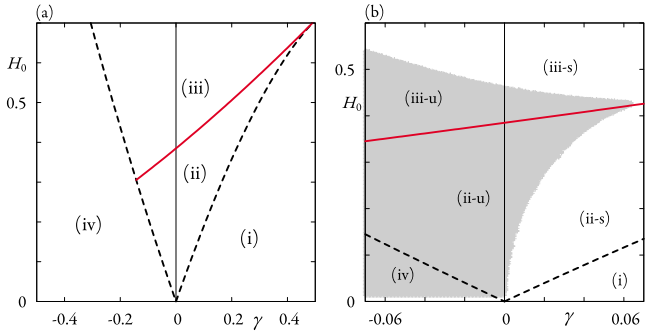

FIG. 1. (Color online) Phase diagram of linearly stable fixed points for $F(t) = \sigma H_0$. Solid line shows $H_0 = H_c(\gamma)$. In (b), the numerically evaluated region satisfying the condition (10) with $\tau_F = 10$ is also shown.

(iii) If $H_0 > -2\gamma\sqrt{1-\gamma}$ and $H_0 > H_c(\gamma)$: One fixed point

$$(\sigma X_3, 0) \tag{8}$$

with $X_3 \equiv \{1/2[H_0 + \sqrt{H_0^2 - H_c^2(\gamma)}]\}^{1/3} + \{1/2[H_0 - \sqrt{H_0^2 - H_c^2(\gamma)}]\}^{1/3}$ exists. At the boundary between (ii) and (iii), two unstable fixed points on $X=0$ disappear by a saddle-node bifurcation.

(iv) If $\gamma < 0$ and $H_0 < -2\gamma\sqrt{1-\gamma}$: One fixed point

$$\left(-\sigma\frac{H_0}{2\gamma}, \frac{\sqrt{4\gamma^2(1-\gamma) - H_0^2}}{2\gamma}\right) \tag{9}$$

exists. At the boundary $H_0 = -2\gamma\sqrt{1-\gamma}$, two stable fixed points are created from a stable fixed point by a pitchfork bifurcation due to the symmetry of $Y \to -Y$.

The four regions (i)–(iv) on the (γ, H_0) plane are presented in Fig. 1(a).

B. Phase diagram on the (γ, H_0) plane

When the system is driven by DMN, the switching never occurs in the region (i) due to the existence of potential barrier. The motion thus belongs to SBM. On the other hand, there exists no potential barrier and the switching occurs in the regions (iii) and (iv). In the region (ii), a potential barrier exists on the line $Y=0$ and, thus, the motion on the line $Y=0$ must be unstable in order for the switching to occur. By the linear stability analysis, the condition reads as

$$\epsilon_I \equiv 1 - \gamma - \langle X_I(t)^2 \rangle > 0 \tag{10}$$

with the solution of Eq. (6), where $\langle \cdots \rangle$ denotes the long-time average. If the condition (10) is not satisfied, $Y=0$ is asymptotically stable and the dynamics is described by Eq. (6) asymptotically. Figure 1(b) shows the numerically evaluated region on the (γ, H_0) plane satisfying the condition (10) for $\tau_F = 10$. Hereafter $\tau_F = 10$ is used in numerical integration of Eqs. (2). The region (ii) splits into (ii-u) and (ii-s) according to the condition (10), as shown in Fig. 1(b). The region (iii) also splits into (iii-u) and (iii-s) in the same manner. The switching, in the region (ii-s), does not occur despite the absence of potential barrier, and the motion results in SBM. In the region (iii-s), the switching along the line $Y=0$ occurs

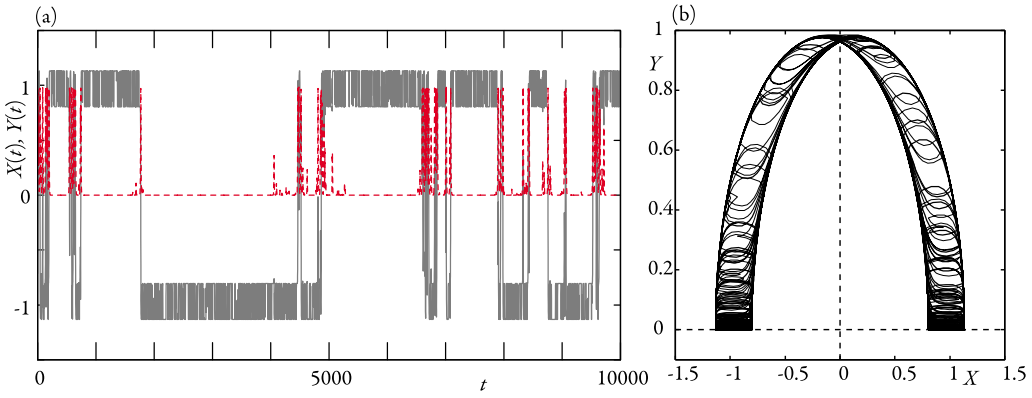

FIG. 2. (Color online) (a) Time series of $X(t)$ (solid line) and $Y(t)$ (dashed line), and (b) $[X(t),Y(t)]$ plot for $\gamma=0.02$ and $H_0=0.3$.

because of $H_0>H_c(\gamma)$, which is called the Ising-type switching whose statistical properties are studied in the previous paper [12]. In the region (ii-u), the condition (10) holds and the switching occurs with a nonzero amplitude of Y avoiding the potential barrier on the line $Y=0$, which is called the Bloch-type switching. As it will be discussed in Sec. IV, both types of the switching occur in the region (iii-u) because $H_0>H_c(\gamma)$ and the condition (10) simultaneously hold.

C. Statistics of Ising-type SRM in the region (iii-s)

In the region (iii-s), $Y=0$ is stable and the dynamics reduces to that of the Ising spin system [12]. The statistics of the Ising-type switching is summarized as follows [12]. Let us denote the time at which the nth switching occurs by t_n $(t_0=0)$, i.e., $X(t_n)=0$, and denote the nth switching time by $\tau_n(=t_n-t_{n-1})$. The switching time is assumed to be an independent identically distributed random variable according to a probability density $\rho_X(\tau)$. By employing the approximation that $|X(t)|\simeq 1$ and $X(t)$ changes its sign at $t=t_n$, the power spectral density (PSD) $I_X(\omega)$ of $X(t)$ is obtained as

$$I_X(\omega)=\frac{4}{\bar{\tau}_X\omega^2}\,\mathrm{Re}\,\frac{1-\tilde{\rho}_X(i\omega)}{1+\tilde{\rho}_X(i\omega)}, \tag{11}$$

where $\bar{\tau}_X$ denotes the average switching time and $\tilde{\rho}_X(z)$ denotes the Laplace transform (LT) of $\rho_X(\tau)$. For large τ compared with a characteristic time τ_{ch} of the system with a constant external field $F(t)=\sigma H_0$, the approximation

$$\rho_X(\tau)\simeq\rho_I(\tau)\equiv\frac{1}{\bar{\tau}_I}e^{-\tau/\bar{\tau}_I} \tag{12}$$

with $\bar{\tau}_X\simeq\bar{\tau}_I\equiv\tau_F e^{\tau_{ch}/\tau_F}$ is valid. The approximation of Eq. (12) leads to

$$I_X(\omega)\simeq\frac{1}{\bar{\tau}_I}\frac{4}{\omega^2+(2/\bar{\tau}_I)^2} \tag{13}$$

for $\omega\gg\tau_{ch}^{-1}$. The formula of Eq. (11) is also used in the following analysis.

III. STATISTICS OF BLOCH-TYPE SRM IN THE REGION (ii-u)

Let us investigate the statistics of the switching by considering PSD determined by Eq. (11) in the region (ii-u). Figure 2 shows a numerically obtained time evolution of Eqs. (2) in this parameter region exhibiting the switching. The figure reveals that the switching of X is associated with the growth of Y, where $Y(t)$ intermittently takes a relatively large value. The state of $0<Y(t)\leqslant Y_c$ is called a laminar state, where Y_c is a small constant proportional to $\sqrt{1-\gamma-\langle X^2\rangle}$ and the nonlinear term in Eq. (2b) can be neglected, and $Y(t)>Y_c$ is a burst state.

It is convenient to rewrite Eq. (2b) as

$$\dot{Y}=[\epsilon_0+f(t)]Y-Y^3 \tag{14}$$

in order to determine the form of $\rho_Y(\tau)$, where $\epsilon_0\equiv 1-\gamma-\langle X(t)^2\rangle$ and $f(t)\equiv\langle X(t)^2\rangle-X(t)^2$ with $\langle f(t)\rangle=0$. In the present parameter region, $\epsilon_0>0$ holds because the condition $\epsilon_0=0$ coincides with the condition $\epsilon_I=0$ due to the fact that Eqs. (2) satisfying $\epsilon_0<0$ reduce to Eq. (6) and $Y=0$. From the behavior of $X(t)$ as shown in Fig. 2, the approximation $f(t)\simeq\pm h_0$ with a constant h_0 holds. As shown in Fig. 3, the probability density $\rho_f(t)$ of the time intervals of $f(t)$, keeping $f(t)>0$ or <0, takes an exponential distribution. Thus, $f(t)$ is approximated by a DMN with effective parameters h_0 and τ_f. It should be noted that Eq. (14) with $f(t)$ replaced by a Gaussian white noise is a well-known stochastic model of on-off intermittency [14,15] and that on-off intermittency is

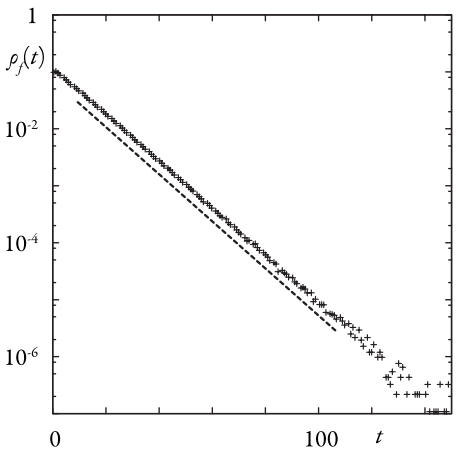

FIG. 3. Probability density $\rho_f(t)$ of the switching time t for $\gamma=0.02$ and $H_0=0.3$. The line shows $\rho_f(t)\propto e^{-t/\tau_f}$ with $\tau_f\simeq 10.5$.

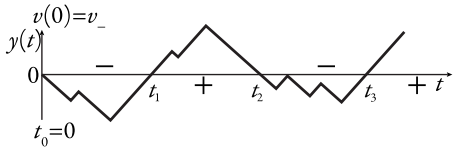

FIG. 4. Schematic sample path of $y(t)$ obeying Eq. (15) with $y(0)=0$. The nth crossing time of $y=0$ is denoted by t_n ($t_0=0$).

also observed in a system driven by the multiplicative DMN [16].

A. Analytical expression of $\rho_Y(\tau)$ and its LT

We derive the probability density $\rho_Y(\tau)$ of laminar length τ obeying Eq. (14) under an assumption that $f(t)$ is a DMN with the amplitude h_0 and the characteristic time τ_f. In the laminar state, the term Y^3 in Eq. (14) can be neglected to give the linearized equation $\dot{Y}=[\epsilon_0+f(t)]Y$, or equivalently

$$\dot{y} = v(t) \equiv \epsilon_0 + f(t) \tag{15}$$

with $y(t) \equiv \ln[Y(t)/Y_c]$. Equation (15) is known as the dichotomous diffusion on a line [11]. Let us consider a sample path $\{y(t); t \geqslant 0\}$ of Eq. (15) with the initial condition $y(0)=0$ as shown in Fig. 4, and regard $y(t)<0$ as laminar state and $y(t)>0$ as a "pseudoburst state." The nonlinear term in Eq. (14) is actually essential for the burst state to be bounded, but it is unnecessary in the following calculation obtaining the distribution of laminar length. Let us assume $y(0)=0$ and introduce $Q_\pm(t)$ defined by

$$Q_\pm(t) \equiv \langle \delta[y(t)] \rangle_{v(0)=v_\pm}, \tag{16}$$

where the average is taken under the condition $v(0)=v_\pm \equiv \epsilon_0 \pm h_0$. Then, as shown in Appendix A, it follows

$$Q_\pm(t) = e^{-t/\tau_f}\delta(v_\pm t) + \frac{e^{-t/\tau_f}}{2h_0\tau_f}\left(I_0(t/\hat{\tau}_f) \mp \frac{v_\mp \hat{\tau}_f}{h_0\tau_f} I_1(t/\hat{\tau}_f) \right), \tag{17}$$

where $\hat{\tau}_f \equiv \tau_f(1-\epsilon^2)^{-1/2}$, $\epsilon \equiv \epsilon_0/h_0$, and $I_\mu(z)$ is the modified Bessel function of the first kind. Furthermore, as shown in Appendix B, $\rho_Y(t)$ satisfies

$$Q_-(t) = |v_-|^{-1}\delta(t) + \int_0^t ds Q_+(s)\rho_Y(t-s), \tag{18}$$

or equivalently

$$\tilde{Q}_-(z) = \frac{1}{h_0 - \epsilon_0} + \tilde{Q}_+(z)\tilde{\rho}_Y\tilde{}(z). \tag{19}$$

Combining Eqs. (17) and (19), we obtain

$$\tilde{\rho}_Y(z) = \frac{\tilde{\rho}_0(\hat{\tau}_f z + \hat{\epsilon}^2/2)}{\tilde{\rho}_0(\hat{\epsilon}^2/2)}, \quad \tilde{\rho}_0(z) \equiv 1 + z - \sqrt{z(z+2)}, \tag{20}$$

with $\hat{\epsilon}^2 \equiv 2[(1-\epsilon^2)^{-1/2}-1]$ and its inverse LT as

$$\rho_Y(\tau) = \tilde{\rho}_0(\hat{\epsilon}^2/2)^{-1}\frac{1}{\tau} I_1\left(\frac{\tau}{\hat{\tau}_f}\right) e^{-\tau/\hat{\tau}_f} \exp\left(-(\hat{\epsilon}^2/2)\frac{\tau}{\hat{\tau}_f}\right). \tag{21}$$

The average laminar length $\bar{\tau}_Y$ is obtained as

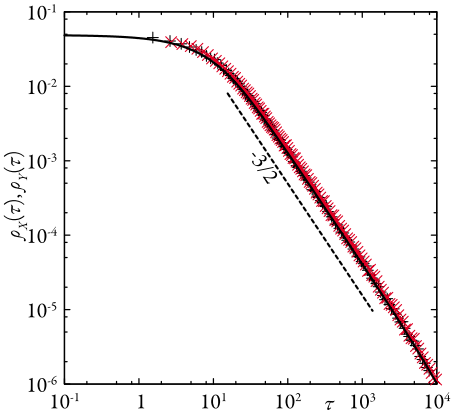

FIG. 5. (Color online) Numerically obtained probability densities $\rho_X(\tau)$ of switching time τ (+) and $\rho_Y(\tau)$ of laminar length τ (×) for $\gamma=0.02$ and $H_0=0.3$ with $Y_c=0.2$. Solid line shows Eq. (21) with $\tau_f=10.5$ and $\epsilon=2.34\times10^{-2}$.

$$\bar{\tau}_Y \equiv \int_0^\infty \tau\rho_Y(\tau)d\tau = -\left.\frac{d}{dz}\tilde{\rho}_Y(z)\right|_{z=0} = \frac{\tau_f}{\epsilon}. \tag{22}$$

Equation (21) is simplified as

$$\rho_Y(\tau) \simeq \frac{1}{2\tilde{\rho}_0(\hat{\epsilon}^2/2)\hat{\tau}_f} \exp\left(-(1+\hat{\epsilon}^2/2)\frac{\tau}{\hat{\tau}_f}\right) \tag{23}$$

for $0<\tau/\hat{\tau}_f \ll 1$ and

$$\rho_Y(\tau) \simeq \frac{1}{\sqrt{2\pi}\tilde{\rho}_0(\hat{\epsilon}^2/2)\hat{\tau}_f}\left(\frac{\tau}{\hat{\tau}_f}\right)^{-3/2} e^{-\hat{\epsilon}^2\tau/2\hat{\tau}_f} \tag{24}$$

for $\tau/\hat{\tau}_f \gg 1$. Equation (24) recovers a well-known form of the laminar length distribution in the on-off intermittency [17].

B. PSD $I_X(\omega)$ and the statistics of $X(t)$

As shown in Appendix C, the distribution function of the switching time of $X(t)$ is approximated by the distribution function of the laminar length, i.e., $\rho_X(t) \simeq \rho_Y(t)$ in the present parameter region. In Fig. 5, the numerically evaluated $\rho_X(\tau)$ and $\rho_Y(\tau)$ are compared with each other, where Eq. (21) with $\tau_f=10.5$ and $\epsilon=2.34\times10^{-2}$ is also shown. The value of effective parameter τ_f is estimated from $\rho_f(t)$ of Fig. 3 and the value of ϵ is determined by using Eq. (22) with a numerical evaluation of $\bar{\tau}_Y$. The result indicates that the statistics of the Bloch-type switching is quite different from that of the Ising-type switching characterized by Eq. (12).

The PSD $I_X(\omega)$ of $X(t)$ is shown in Fig. 6, where the analytical expression obtained by substituting Eq. (20) into Eq. (11) with the assumption $\tilde{\rho}_X(z) \simeq \tilde{\rho}_Y(z)$ is compared with the numerical result. The PSD $I_X(\omega)$ consists of three regions that are classified as follows:

(i) $I_X(\omega) \simeq$ const for $0<\omega<\hat{\epsilon}^2/2\hat{\tau}_f$,
(ii) $I_X(\omega) \propto \omega^{-3/2}$ for $\hat{\epsilon}^2/2\hat{\tau}_f < \omega < \hat{\tau}_f^{-1}$,
(iii) $I_X(\omega) \propto \omega^{-2}$ for $\hat{\tau}_f^{-1} < \omega$

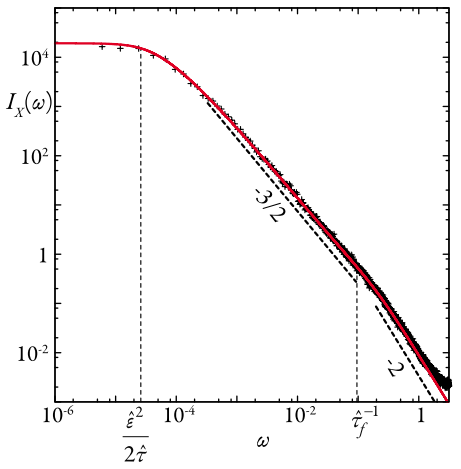

FIG. 6. (Color online) PSD for $\gamma=0.02$, $H_0=0.3$, and $\tau_F=10$. Solid line is the result of Eq. (20) with Eq. (11) under the assumption $\tilde{\rho}_X(z)\simeq\tilde{\rho}_Y(z)$, where the values of ϵ and τ_f are the same as those in Fig. 5.

The behavior in (ii), which is quite different from that of the Ising-type switching given by Eq. (13), implies that the correlation function of $X(t)$ depends on time in a stretched exponential way as [18]

$$\langle X(0)X(t)\rangle \propto e^{-C\sqrt{t}} \tag{25}$$

with a constant C.

Each behavior of $I_X(\omega)$ in the three regions of ω is explained as follows: (i) $\tilde{\rho}_X(i\omega)$ for $0<\hat{\tau}_f\omega\ll\hat{\epsilon}^2/2$ is expanded as

$$\tilde{\rho}_X(i\omega)=1-\alpha_1\hat{\tau}_f\omega i-\alpha_2(\hat{\tau}_f\omega)^2+O[(\hat{\tau}_f\omega)^3], \tag{26}$$

where $\alpha_1\equiv 1/\sqrt{a(a+2)}$ and $\alpha_2\equiv\frac{1+a+\sqrt{a(a+2)}}{2[a(a+2)]^{3/2}}$ with $a\equiv\hat{\epsilon}^2/2$. Substitution of Eq. (26) into Eq. (11) yields

$$I_X(\omega)=\frac{\tau_f}{\epsilon^2}. \tag{27}$$

(ii) $\tilde{\rho}_X(i\omega)$ for $\hat{\epsilon}^2/2\ll\hat{\tau}_f\omega\ll 1$ is then expanded, by setting $\hat{\epsilon}^2/2=0$, as

$$\tilde{\rho}_X(i\omega)\simeq\tilde{\rho}_0(i\hat{\tau}_f\omega)=1-\sqrt{\hat{\tau}_f\omega}-(\sqrt{\hat{\tau}_f\omega}-\hat{\tau}_f\omega)i+O[(\hat{\tau}_f\omega)^{3/2}], \tag{28}$$

which yields

$$I_X(\omega)=\frac{2\epsilon}{\sqrt{\tau_f}}\omega^{-3/2}+O(\omega^{-1}). \tag{29}$$

(iii) In the case of $\hat{\tau}_f\omega\gg 1$, the expansion

$$\tilde{\rho}(i\omega)\simeq 1+i\hat{\tau}_f\omega-i\hat{\tau}_f\omega\sqrt{1-2i(\hat{\tau}_f\omega)^{-1}} \tag{30}$$

with

$$\sqrt{1-2i(\hat{\tau}_f\omega)^{-1}}\simeq 1-i(\hat{\tau}_f\omega)^{-1}+\tfrac{1}{2}(\hat{\tau}_f\omega)^{-2}+\tfrac{1}{2}(\hat{\tau}_f\omega)^{-3}i+O[(\hat{\tau}_f\omega)^{-4}] \tag{31}$$

leads to

$$I_X(\omega)\simeq\frac{4\epsilon}{\tau_f}\omega^{-2}. \tag{32}$$

C. Scaling functions of PSDs for $X(t)$ and $Y(t)$

We here investigate the scaling properties of the PSDs of $X(t)$ and $Y(t)$. Let us first consider a normalized time series $\{N[Y(t)]\}$ by using a function

$$N(x)\equiv\begin{cases}0, & x\leqslant Y_c,\\ 1, & x>Y_c.\end{cases} \tag{33}$$

The probability density $\rho_Y(\tau)$ of laminar length and its LT $\tilde{\rho}_Y(z)$ are given by Eqs. (21) and (20), respectively. Let $\tilde{\rho}_b(z)$ be LT of the probability density $\rho_b(\tau)$ of burst length. Then the PSD $I_Y(\omega)$ of $N[Y(t)]$ is expressed as

$$I_Y(\omega)\equiv\lim_{T\to\infty}\frac{1}{T}\left|\int_0^T N[Y(t)]e^{-i\omega t}dt\right|^2 \tag{34}$$

$$=\frac{2}{\bar{\tau}_Y\omega^2}\,\mathrm{Re}\,\frac{[1-\tilde{\rho}_Y(i\omega)][1-\tilde{\rho}_b(i\omega)]}{1-\tilde{\rho}_X(i\omega)\tilde{\rho}_b(i\omega)}, \tag{35}$$

which is derived in the same way as in Ref. [13].

For simplicity let us assume that $\rho_b(\tau)$ is an exponential distribution $\rho_b(\tau)=\tau_b^{-1}e^{-\tau/\tau_b}$, or equivalently

$$\tilde{\rho}_b(z)=\frac{1}{1+\tau_b z}, \tag{36}$$

where τ_b is the average length of burst state. Then $I_Y(\omega)$ in the limit $\epsilon\to 0$ ($\bar{\tau}_Y\to\infty$) satisfies a scaling relation

$$I_Y(\omega)=\frac{\tau_b^2}{\tau_f}f_Y\left(\frac{2\bar{\tau}_Y^2\omega}{\tau_f}\right) \tag{37}$$

as shown in Appendix D, where the scaling function $f_Y(x)$ is given by

$$f_Y(x)=\frac{\sqrt{2}}{\sqrt{1+\sqrt{1+x^2}}}. \tag{38}$$

The scaled plots of numerically evaluated PSDs of $Y(t)$ for $\gamma=0.015$, 0.02, and 0.023 with $H_0=0.3$ are compared with the scaling function $f_Y(x)$ in Fig. 7, where the scaled plots of Eq. (35) are also shown. Since the value of effective parameter τ_f is almost unchanged for these parameter values as well as τ_b, the same values $\tau_f=10.5$ and $\tau_b=14$ are used in Fig. 7, where the value of τ_b is estimated from the numerically generated $\rho_b(\tau)$. It is confirmed that the scaling of Eq. (37) with Eq. (38) holds in the limit $\bar{\tau}_Y\to\infty$. The form of Eq. (38) in the context of the on-off intermittency has been derived by using a multiplicative noise system [19], a piecewise linear map [20], and the continuous-time random walk theory [21]. The fact that PSD in the system driven by DMN also obeys the same scaling function ensures that the on-off intermittency is generally characterized by Eq. (38).

Next let us consider the PSD $I_X(\omega)$ of $X(t)$, which is approximately obtained by Eq. (11) with the assumption $\tilde{\rho}_X(z)\simeq\tilde{\rho}_Y(z)$, as mentioned above. It is shown in Appendix

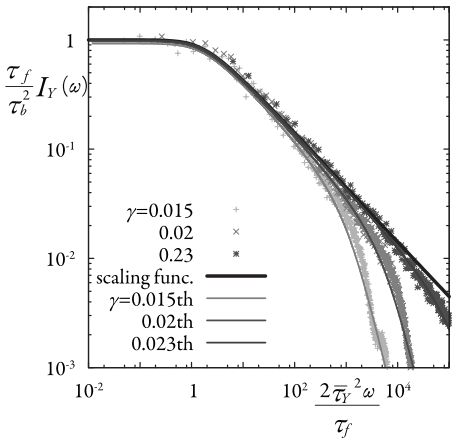

FIG. 7. Scaled plots of PSDs of $Y(t)$ for γ=0.015, 0.02, and 0.023 with H_0=0.3. Black line shows Eq. (38). Gray lines show the results of Eq. (35) with τ_f=10.5 and τ_b=14. The values of the average laminar length are $\overline{\tau}_Y$=2.08×10^2, 4.82×10^2, and 2.36×10^3 for γ=0.015, 0.02, and 0.023, respectively.

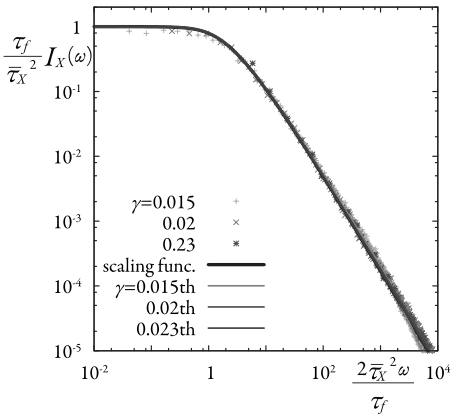

FIG. 8. Scaled plots of PSDs of $X(t)$ for γ=0.015, 0.02, and 0.023 with H_0=0.3. Black line shows Eq. (40). Gray lines show the results of Eq. (11) with τ_f=10.5. The values of the average switching time are $\overline{\tau}_X$=1.90×10^2, 4.48×10^2, and 2.27×10^3 for γ=0.015, 0.02, and 0.023, respectively.

D that $I_X(\omega)$ in the limit $\epsilon \to 0$ ($\overline{\tau}_X \to \infty$) satisfies a scaling relation

$$I_X(\omega) = \frac{\overline{\tau}_X^2}{\tau_f} f_X\left(\frac{2\overline{\tau}_X^2 \omega}{\tau_f}\right), \tag{39}$$

where the scaling function $f_X(x)$ is given by

$$f_X(x) = \frac{4\sqrt{2}}{(1+\sqrt{1+x^2})(\sqrt{1+\sqrt{1+x^2}}+\sqrt{2})}. \tag{40}$$

Figure 8 compares the scaled plots of numerically evaluated $I_X(\omega)$ and Eq. (11) for several parameter values with the scaling function $f_Y(x)$. It is confirmed that the scaling of Eq. (39) holds in the limit $\overline{\tau}_X \to \infty$.

IV. STATISTICS OF SRM IN THE REGION (iii-u)

Let us investigate the statistics of the switching in the region (iii-u). In this parameter region, the Ising-type switching characterized by the probability density $\rho_I(\tau)$ occurs because the condition $H_0 > H_c(\gamma)$ is satisfied. Moreover, the Bloch-type switching characterized by the probability density $\rho_Y(\tau)$, under the approximation that each burst of $Y(t)$ corresponds to a switching of $X(t)$ that is expressed as $\rho_X(\tau) \simeq \rho_Y(\tau)$ in the preceding section, also occurs because the condition (10) is satisfied. As a result, there coexist both types of the switching in the present parameter region. In fact, Fig. 9 shows that the switching occurs both with $Y \geqslant Y_c$ (the Bloch-type switching) and with $Y \simeq 0$ (the Ising-type switching). The probability density $\rho_X(\tau)$ of switching time τ is thus characterized by neither $\rho_I(\tau)$ nor $\rho_Y(\tau)$, as shown in Fig. 10. Since the rate of the Ising-type switching becomes small (large) for $0 < H_0 - H_c(\gamma) \ll 1$ [$H_0 - H_c(\gamma) \gg 0$], $\rho_X(\tau)$ agrees with $\rho_Y(\tau)$ [$\rho_I(\tau)$] in the limit $H_0 \to H_c(\gamma)$ [$H_0 \gg H_c(\gamma)$].

We attempt to determine the analytical form of $I_X(\omega)$ by assuming that the Ising-type switching and the Bloch-type switching occur independently, with the approximation that each burst of $Y(t)$ corresponds to a switching of Bloch type. The probabilities $\Xi_I(\tau)$ and $\Xi_Y(\tau)$ that the switchings do not occur in a time interval τ are defined by

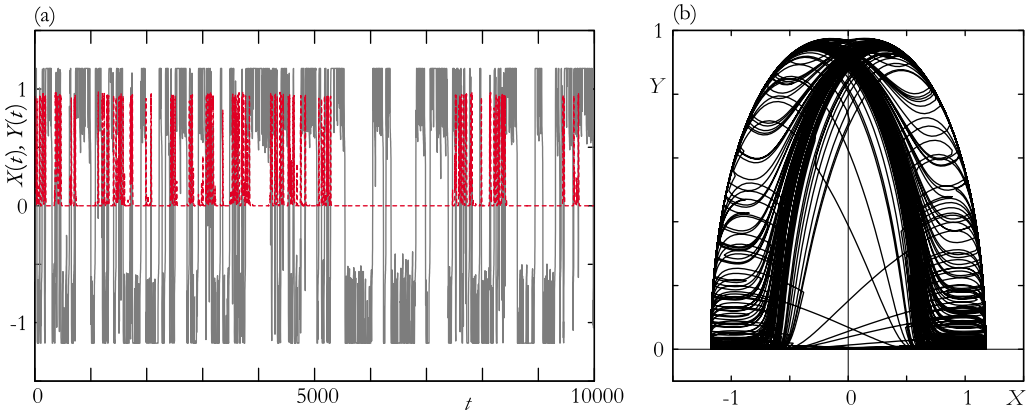

FIG. 9. (Color online) (a) Time series of $X(t)$ (solid line) and $Y(t)$ (dashed line), and (b) ($X(t)$, $Y(t)$) plot for γ=0.03 and H_0=0.415.

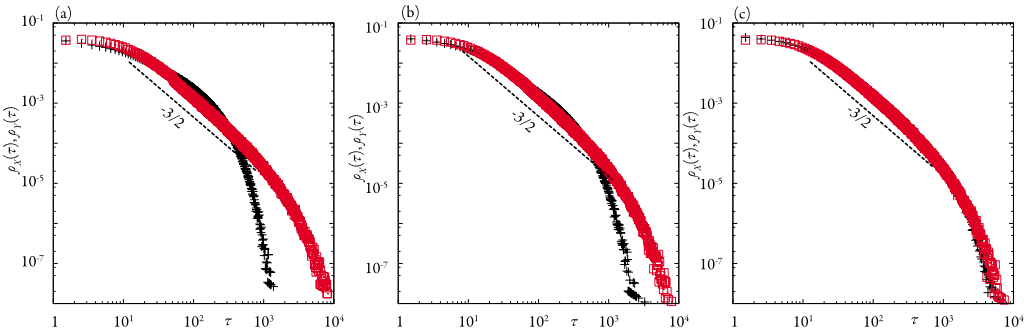

FIG. 10. (Color online) The probability densities $\rho_X(\tau)$ (+) and $\rho_Y(\tau)$ (□) for (a) H_0=0.415, (b) 0.41, and (c) 0.405 with γ=0.03, where $H_c \simeq 0.402$.

$$\Xi_{I(Y)}(\tau) \equiv \int_{\tau}^{\infty} \rho_{I(Y)}(s)ds. \tag{41}$$

The assumption leads the whole probability $\Xi_X(\tau)$ that the switching does not occur in a time interval τ to

$$\Xi_X(\tau) = \Xi_I(\tau)\Xi_Y(\tau) = e^{-\pi/\bar{\tau}_I}\Xi_Y(\tau), \tag{42}$$

where it is assumed that each burst in $Y(t)$ corresponds to a switching of $X(t)$. Then the probability density $\rho_X(\tau)$ of the switching time τ in the present parameter region is obtained as

$$\rho_X(\tau) = -\frac{d}{d\tau}\Xi_X(\tau). \tag{43}$$

Applying LT to Eq. (43) yields

$$\tilde{\rho}_X(z) = 1 - z\tilde{\Xi}_X(z) = 1 - \frac{z}{z+\bar{\tau}_I^{-1}}[1-\tilde{\rho}_Y(z+\bar{\tau}_I^{-1})], \tag{44}$$

where LT of Eq. (42), $\tilde{\Xi}_X(z)=[1-\tilde{\rho}_Y(z+\bar{\tau}_I^{-1})]/(z+\bar{\tau}_I^{-1})$, is used. Substitution of Eq. (44) into Eq. (11) gives the analytical form of $I_X(\omega)$ in the region (iii-u).

Figures 11 and 12 show both the analytical and numerical results of $I_X(\omega)$ for two parameter values satisfying $\hat{\epsilon}^2/2\hat{\tau}_f > \bar{\tau}_I^{-1}$ (Fig. 11) and $\hat{\epsilon}^2/2\hat{\tau}_f < \bar{\tau}_I^{-1}$ (Fig. 12). The effective parameters τ_f and ϵ in Eq. (20) are evaluated in the same manner as mentioned in Sec. III A. On the other hand, $\bar{\tau}_I$ in Eq. (12) is evaluated in terms of Eq. (6) using the same values of γ and H_0. The average switching time $\bar{\tau}_X$ in Eq. (11) is determined from

$$\bar{\tau}_X = -\left.\frac{d\tilde{\rho}_X(z)}{dz}\right|_{z=0} = [1-\tilde{\rho}_Y(\bar{\tau}_I^{-1})]\bar{\tau}_I. \tag{45}$$

These figures show that $I_X(\omega)$ in the present parameter region also consists of three regions as discussed in Sec. III, and that $I_X(\omega) \propto \omega^{-3/2}$ holds for $\max(\bar{\tau}_I^{-1}, \hat{\epsilon}^2/2\hat{\tau}_f) < \omega < \bar{\tau}_f^{-1}$. The result reveals that the correlation function of $X(t)$ in the present parameter region is also characterized by Eq. (25) in an intermediate time scale.

The dependence of $I_X(\omega)$ on ω is analytically determined as follows. $\tilde{\rho}_X(i\omega)$ for $0 < \bar{\tau}_I\omega \ll 1$ is expanded as

$$\tilde{\rho}_X(i\omega) = 1 - i\alpha_1\bar{\tau}_I\omega - \alpha_2(\bar{\tau}_I\omega)^2 + O[(\bar{\tau}_I\omega)^3], \tag{46}$$

where α_1 and α_2 are defined by

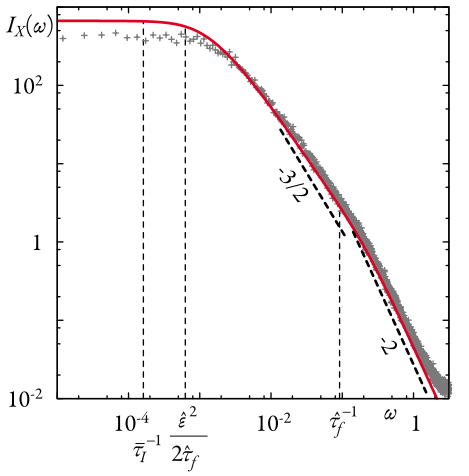

FIG. 11. (Color online) PSD for γ=0.025, H_0=0.401, and τ_F =10. The solid line shows theoretical results with $\epsilon \simeq 1.17\times10^{-1}$, $\tau_f \simeq 10.9$, and $\bar{\tau}_I \simeq 6190$.

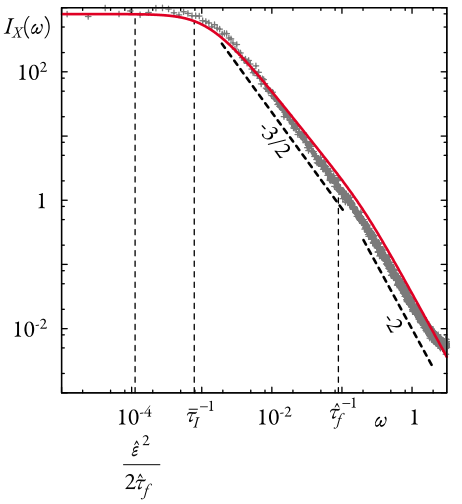

FIG. 12. (Color online) PSD for γ=0.05, H_0=0.417, and τ_F =10. The solid line shows theoretical results with $\epsilon \simeq 4.21\times10^{-2}$, $\tau_f \simeq 11.2$, and $\bar{\tau}_I \simeq 1280$.

$$\alpha_1 \equiv 1 - \tilde{\rho}_Y(\bar{\tau}_I^{-1}), \quad \alpha_2 \equiv 1 - \left(1 + \frac{\hat{\tau}_f \bar{\tau}_I^{-1}}{\sqrt{a(a+2)}}\right)\tilde{\rho}_Y(\bar{\tau}_I^{-1}) \tag{47}$$

with $a \equiv \hat{\tau}_f \bar{\tau}_I^{-1} + \hat{\epsilon}^2/2$. The substitution of Eq. (46) into Eq. (11) yields

$$I_X(\omega) = \frac{2\alpha_2 - \alpha_1^2}{\alpha_1}\bar{\tau}_I, \tag{48}$$

where $\bar{\tau}_X = \alpha_1 \bar{\tau}_I$ is used. In the case of $\bar{\tau}_I \omega \gg 1$, whereas, one can set $\bar{\tau}_I^{-1} = 0$ in Eq. (44) and thus $\tilde{\rho}_X(z) = \tilde{\rho}_Y(z)$ holds. As a result, the PSD for $\bar{\tau}_I^{-1} \ll \omega$ agrees with the PSD in the region (ii-u) described in Sec. III A.

The dependence of $I_X(\omega)$ on ω is summarized as follows. If $\hat{\epsilon}^2/2\hat{\tau}_f \ll \bar{\tau}_I^{-1}$ is satisfied, then Eq. (48) with $\hat{\epsilon}=0$ reduces to $I_X(\omega) = \bar{\tau}_I$ for $\omega \ll \bar{\tau}_I^{-1}$. In the case of $\bar{\tau}_I^{-1} \ll \hat{\epsilon}^2/2\hat{\tau}_f$, on the other hand, the approximation $\bar{\tau}_I = 0$ in Eq. (44) eventually yields Eq. (27) for $\omega \ll \hat{\epsilon}^2/2\hat{\tau}_f$. The asymptotic forms of the PSD for $\max(\bar{\tau}_I^{-1}, \hat{\epsilon}^2/2\hat{\tau}_f) \ll \omega \ll \hat{\tau}_f^{-1}$ and for $\hat{\tau}_f^{-1} \ll \omega$ are given by Eqs. (29) and (32), respectively.

V. CONCLUDING REMARKS

In this paper, we have investigated the statistics of a subcritical spatially homogeneous XY spin system driven by symmetric dichotomous Markov noise (DMN) as an external field, particularly focusing on the switching process of parallel component $X(t)$ to the external field, which restores the symmetry of the system. The motion of $X(t)$ is classified according to whether the switching process occurs or not, and the transition between the two types of motions can be observed by changing the amplitude of the DMN. The switching process is, moreover, classified into three types called the Ising-type switching, the Bloch-type switching, and the mixture of both types.

The probability density $\rho_X(\tau)$ of switching time τ and the power spectral density (PSD) $I_X(\omega)$ of $X(t)$ for the Bloch-type switching are formulated by making use of the fact that the dynamics of perpendicular component $Y(t)$ to the direction of DMN, exhibits on-off intermittency. It is revealed that $I_X(\omega)$ depends on ω as

$$I_X(\omega) \propto \omega^{-3/2} \tag{49}$$

in an intermediate range of ω, thus that the correlation function $\langle X(0)X(t)\rangle$ is characterized by a stretched exponential form $e^{-C\sqrt{t}}$ with a constant C. The scaling functions of the PSD $I_X(\omega)$ of $X(t)$ and that of $Y(t)$ are also derived.

Then the statistics of the switching processes in the mixture of Ising and Bloch types is discussed under an assumption that each process occurs independently. It is shown that $I_X(\omega)$ also takes the form of $I_X(\omega) \propto \omega^{-3/2}$ in an intermediate range of ω, and its condition is determined.

ACKNOWLEDGMENTS

The authors would like to thank Hiroki Hata, Per Arne Rikvold, Ulrich Behn, and Arkady Pikovsky for valuable discussions. This study was partially supported by the 21st Century COE Program "Center Of Excellence for Research and Education on Complex Functional Mechanical Systems" at Kyoto University.

APPENDIX A: EXPLICIT FORM OF $Q_\pm(t)$

By integrating Eq. (15), Eq. (16) is rewritten as

$$Q_\pm(t) = \langle \delta[\epsilon_0 t + W(t)]\rangle_{f(0)=\pm h_0} \tag{A1}$$

with $W(t) = \int_0^t f(s)ds$. By introducing

$$P_\pm(w, \alpha; t) = \langle \delta[w - W(t)]\delta_{f(t),\alpha}\rangle_{f(0)=\pm h_0}, \tag{A2}$$

which satisfies the initial condition $P_\pm(w, \alpha; 0) = \delta(w)\delta_{\alpha,\pm h_0}$, $Q_\pm(t)$ is expressed as

$$Q_\pm(t) = P_\pm(-\epsilon_0 t, +h_0; t) + P_\pm(-\epsilon_0 t, -h_0; t). \tag{A3}$$

Since $\dot{W}(t) = f(t)$, $P_\pm(w, \alpha; t)$ satisfies the master equation [10]

$$\partial_t P(+h_0) = -h_0 \partial_w P(+h_0) + \tau_f^{-1}[P(-h_0) - P(+h_0)], \tag{A4a}$$

$$\partial_t P(-h_0) = h_0 \partial_w P(-h_0) + \tau_f^{-1}[P(+h_0) - P(-h_0)], \tag{A4b}$$

where the abbreviation $P(\alpha) = P_\pm(w, \alpha; t)$ is used. Equations (A4) with any initial conditions can be solved analytically [22], and we obtain

$$\begin{aligned} &P_\pm(w, +h_0; t) + P_\pm(w, -h_0; t) \\ &\quad = e^{-t/\tau_f}\delta(w \mp h_0 t) \\ &\quad + \frac{e^{-t/\tau_f}}{2h_0\tau_f}\left(I_0(\xi/h_0\tau_f) + \frac{h_0 t \pm w}{\xi} I_1(\xi/h_0\tau_f)\right) \\ &\quad \times [\theta(w + h_0 t) - \theta(w - h_0 t)]. \end{aligned} \tag{A5}$$

Here $\xi \equiv \sqrt{h_0^2 t^2 - w^2}$ is introduced, and $I_\mu(z)$ and $\theta(x)$ denote the modified Bessel function of the first kind and the Heaviside function, respectively. Finally, substitution of Eq. (A5) into Eq. (A3) yields Eq. (17).

APPENDIX B: RELATION BETWEEN $Q_\pm(t)$ AND $\rho_Y(t)$

Let us consider a sample path $\{y(t); t \geq 0\}$ of Eq. (20) satisfying $y(0) = 0$ and assume that the ith crossing of $y = 0$ takes place at $t = t_i$ ($t_0 = 0$) i.e., $y(t_i) = 0$. See Fig. 4. For almost all paths, either $v(t_i) = v_-$ or $v(t_i) = v_+$ holds, because the probability that the DMN $f(t)$ changes its sign at a given time $t = t_i$ is zero. Thus, for almost all paths satisfying $v(0) = v_-$, $v(t_1) = v_+$ holds and we have

$$Q_+(t) = \langle \delta[y(t + t_1)]\rangle_{v(0)=v_-}. \tag{B1}$$

Since $y(t) = y(t_i + t - t_i) \to v(t_i)(t - t_i)$ for $t \to t_i$, we obtain

$$\delta[y(t)] = \sum_{i=0}^{\infty} \delta[v(t_i)(t-t_i)] \tag{B2}$$

$$= |v(0)|^{-1}\delta(t) + \sum_{i=0}^{\infty} \delta[v(t_{i+1})(t-t_{i+1})] \tag{B3}$$

$$= |v(0)|^{-1}\delta(t) + \int_0^t ds \sum_{i=0}^{\infty} \delta[v(t_{i+1}) \times (s+t_1-t_{i+1})]\delta(s-t+t_1) \tag{B4}$$

$$= |v(0)|^{-1}\delta(t) + \int_0^t ds\, \delta[y(s+t_1)]\delta(t-s-t_1) \tag{B5}$$

for almost all paths, where

$$\delta[y(t+t_1)] = \sum_{i=0}^{\infty} \delta[v(t_{i+1})(t+t_1-t_{i+1})] \tag{B6}$$

$(t \geqslant 0)$ is used. Taking the average under the condition $v(0) = v_-$, Eq. (B5) leads to

$$Q_-(t) = |v_-|^{-1}\delta(t) + \int_0^t ds \langle \delta[y(s+t_1)]\delta(t-s-t_1)\rangle_{v(0)=v_-} \tag{B7}$$

$$= |v_-|^{-1}\delta(t) + \int_0^t ds \langle \delta[y(s+t_1)]\rangle_{v(0)=v_-} \times \langle \delta(t-s-t_1)\rangle_{v(0)=v_-}, \tag{B8}$$

since t_1 and $y(s+t_1)$ $(s \geqslant 0)$ are statistically independent of each other. With Eq. (B1) and the identity

$$\rho_Y(t) = \langle \delta(t-t_1)\rangle_{v(0)=v_-} = \langle \delta[t-(t_{2j+1}-t_{2j})]\rangle_{v(0)=v_-} \quad (j=0,1,2,\ldots), \tag{B9}$$

Eq. (B8) reads as Eq. (18).

APPENDIX C: RELATION BETWEEN $\rho_X(x)$ AND $\rho_Y(x)$

Let us consider the relation between the distribution function of the switching time of $X(t)$ and that of the laminar length of $Y(t)$, in the Bloch-type switching. The region of laminar state $0 \leqslant Y < Y_c$ on the XY plane is divided into the left laminar region (LLR) and the right laminar region (RLR) according to the sign of X. The region $Y > Y_c$ is denoted as the transition region (TR) that corresponds to the burst state. Here we define the switching of X as the event that starting from a given state point in LLR or RLR the orbit arrives at the other side of the laminar region for the first time. Note that in the main text the switching is defined as the crossing of $X=0$, which takes place in TR in the Bloch-type switching. Here, we employ the above definition for the simplicity of formulation. The two definitions coincide, if multiple crossings of $X=0$ in TR is neglected. Note also that the contribution of the multiple crossing to the power spectral density $I_X(\omega)$ of $X(t)$ is relatively small, because it takes place around $X=0$.

Prior to each switching the state point visits TR. The probability density of the residence time in TR is expressed as a sum of two parts: One denoted by $\rho_T(\tau)$ is that for the orbit segments connecting LLR and RLR, which corresponds to switching, and the other denoted by $\rho^*(\tau)$ is that for the orbit segments connecting the same region of LLR or RLR. For $\rho_T(\tau)$, the minimum τ^* of τ satisfying $\rho_T(\tau) > 0$ exits, which is a characteristic relaxation time of the dynamics under fixed $F(t) = \sigma H_0$. Let $\Xi_X(\tau)$ be the probability that switching time is greater than τ, i.e.,

$$\Xi_X(\tau) = \int_\tau^\infty ds \rho_X(s), \tag{C1}$$

and $\Xi_Y(\tau)$ be that of the laminar length. Noting $\rho_X(\tau)=0$ for $\tau < \tau^*$ and extracting the initial laminar state from the process of switching, the following relation for $\tau \geqslant \tau^*$ is obtained,

$$\Xi_X(\tau) = \Xi_Y(\tau-\tau^*) + \int_0^{\tau-\tau^*} ds \int_0^{\tau-\tau^*-s} ds' \rho_Y(s)\rho^*(s')\Xi_X \times (\tau-s-s'). \tag{C2}$$

By differentiating with respect to τ, Eq. (C2) is transformed into

$$\rho_X(\tau) = \rho_Y(\tau-\tau^*) - \int_0^{\tau-\tau^*} ds \rho_Y(s)\rho^*(\tau-\tau^*-s) + \int_0^{\tau-\tau^*} ds \int_0^{\tau-\tau^*-s} ds' \rho_Y(s)\rho^*(s')\rho_X(\tau-s-s'), \tag{C3}$$

where $\Xi_X(\tau^*)=1$ is used. By performing LT, Eq. (C3) is solved for $\tilde{\rho}_X(z)$ as

$$\tilde{\rho}_X(z) = e^{-z\tau^*}\tilde{\rho}_Y(z)\frac{1-\tilde{\rho}^*(z)}{1-\tilde{\rho}^*(z)\tilde{\rho}_X(z)}. \tag{C4}$$

By definition, $\rho^*(\tau)$ is not normalized, but satisfies

$$\int_0^\infty d\tau \rho^*(\tau) + \int_{\tau^*}^\infty d\tau \rho_T(\tau) = 1. \tag{C5}$$

On the other hand, the probability that $F(t)$ does not change its sign for a time interval of τ^* is given by $\int_{\tau^*}^\infty p(\tau)d\tau = e^{-\tau^*/\tau_F}$, which implies $\rho_T(\tau)$ contains $e^{-\tau^*/\tau_F}\delta(\tau-\tau^*)$ as its component. Thus, we obtain

$$p^* \equiv \tilde{\rho}^*(0) = \int_0^\infty d\tau \rho^*(\tau) < 1 - e^{-\tau^*/\tau_F}. \tag{C6}$$

If p^* is sufficiently small, which is deduced from Eq. (C6) for small τ^*/τ_F, then the terms of $\tilde{\rho}^*(z)$ in Eq. (C4) are negligible, i.e., $\tilde{\rho}_Y(z) \simeq e^{-\tau^* z}\tilde{\rho}_Y(z)$. This leads to $\rho_X(\tau)$

$\simeq \rho_Y(\tau-\tau^*)$ and $\rho_X(\tau)\simeq\rho_Y(\tau)$ for large τ. Even if p^* is not small, the following justification for the approximation of $\rho_X(\tau)\simeq\rho_Y(\tau)$ can be made. We are interested in $\rho_X(\tau)$ for large τ, where the power-law behavior is expected. For $\rho_Y(\tau)$ exhibiting the power-law behavior, we have $|1-\tilde{\rho}_Y(z)| = O(\sqrt{|z|})$ for sufficiently small $|z|$, which leads to

$$\frac{1-\tilde{\rho}^*(z)}{1-\tilde{\rho}^*(z)\tilde{\rho}_Y(z)} = 1 - \frac{\tilde{\rho}^*(z)}{1-\tilde{\rho}^*(z)} O(\sqrt{|z|}), \tag{C7}$$

and thus $\tilde{\rho}_X(z)\simeq\tilde{\rho}_Y(z)$.

APPENDIX D: SCALING FUNCTIONS $f_X(x)$ AND $f_Y(x)$

Let us show that the scaling functions $f_X(x)$ of $I_X(\omega)$ and $f_Y(x)$ of $I_Y(\omega)$ are given by Eqs. (40) and (38), respectively. By introducing the decomposition $1-\tilde{\rho}_Y(i\omega)=L_R+iL_I$ and $1-\tilde{\rho}_b(i\omega)=B_R+iB_I$ into real and imaginary parts, $I_X(\omega)$ and $I_Y(\omega)$ are written in the following forms:

$$I_X(\omega) = \frac{4}{\bar{\tau}_X\omega^2}\frac{2L_R-(L_R^2+L_I^2)}{4-4L_R+(L_R^2+L_I^2)}, \tag{D1}$$

$$I_Y(\omega) = \frac{2}{\bar{\tau}_Y\omega^2}\frac{X(R-X)+Y(I-Y)}{(R-X)^2+(I-Y)^2}, \tag{D2}$$

respectively, where $R=B_R+L_R$, $I=B_I+L_I$, $X=L_RB_R-L_IB_I$, and $Y=L_IB_R+L_RB_I$ are introduced. One finds that

$$B_R = \frac{(\tau_b\omega)^2}{1+(\tau_b\omega)^2}, \quad B_I = \frac{\tau_b\omega}{1+(\tau_b\omega)^2}. \tag{D3}$$

The explicit forms of L_R and L_I are, on the other hand, obtained as follows. Equation (20) takes the form

$$\tilde{\rho}_Y(i\omega) = (1-\epsilon)^{-1}[1+i\tau_f\omega-\sqrt{\epsilon^2-(\tau_f\omega)^2+2i\tau_f\omega}] \tag{D4}$$

by replacing $\hat{\epsilon}$ and $\hat{\tau}_f$ to the original parameters $\epsilon = \sqrt{1-(1+\hat{\epsilon}^2/2)^{-2}}$ and $\tau_f=\hat{\tau}_f(1-\epsilon^2)^{1/2}$. By using r and θ defined by $\epsilon^2-(\tau_f\omega)^2+2i\tau_f\omega\equiv re^{i\theta}$, one finds that

$$L_R = (1-\epsilon)^{-1}(\sqrt{r+r\cos\theta}/\sqrt{2}-\epsilon), \tag{D5}$$

$$L_I = (1-\epsilon)^{-1}(\sqrt{r-r\cos\theta}/\sqrt{2}-\tau_f\omega),$$

where

$$r = \sqrt{[\epsilon^2-(\tau_f\omega)^2]^2+4(\tau_f\omega)^2}, \quad r\cos\theta = \epsilon^2-(\tau_f\omega)^2. \tag{D6}$$

Let us introduce the scaling variable x defined by $x \equiv 2\tau_f\omega/\epsilon^2$. Then Eqs. (D3) are expanded as

$$B_R = \epsilon^4\hat{B}^2+O(\epsilon^8), \quad B_I = \epsilon^2\hat{B}+O(\epsilon^6) \tag{D7}$$

with

$$\hat{B} \equiv \frac{\tau_b}{2\tau_f}x. \tag{D8}$$

Furthermore, Eqs. (D6) are expanded as

$$r = \epsilon^2\sqrt{1+x^2}+O(\epsilon^4), \quad r\cos\theta = \epsilon^2+O(\epsilon^4), \tag{D9}$$

which yield

$$L_R = \epsilon\hat{L}_R+\epsilon^2\hat{L}_R+O(\epsilon^3), \quad L_I = \epsilon\hat{L}_I-\epsilon^2(x/2-\hat{L}_I)+O(\epsilon^2) \tag{D10}$$

with

$$\hat{L}_R \equiv \frac{1}{\sqrt{2}}(\sqrt{\sqrt{1+x^2}+1}-\sqrt{2}), \quad \hat{L}_I \equiv \frac{1}{\sqrt{2}}\sqrt{\sqrt{1+x^2}-1}. \tag{D11}$$

Equation (D2) is eventually expanded as

$$I_Y(\omega) = \frac{2}{\bar{\tau}_Y\omega^2}\frac{\epsilon^3\hat{L}_R\hat{B}^2}{\hat{L}_R^2+\hat{L}_I^2}+O(\epsilon^4) \tag{D12}$$

by substituting Eqs. (D7) and (D10). Substitution of Eqs. (D8) and (D11) and $\epsilon=\tau_f/\bar{\tau}_Y$ into Eq. (D12) yields Eq. (37) with Eq. (38) in the limit $\epsilon\to 0$. On the other hand, Eq. (D1) is expanded as

$$I_X(\omega) = \frac{2\epsilon}{\bar{\tau}_X\omega^2}\hat{L}_R+O(\epsilon^2) \tag{D13}$$

by substituting Eq. (D10). Equation (D13) with $\hat{L}_R$ in Eq. (D11) and $\epsilon=\tau_f/\bar{\tau}_X$ leads to Eq. (39) with Eq. (40).

[1] T. Tomé and M. J. de Oliveira, Phys. Rev. A **41**, 4251 (1990); J. F. F. Mendes and E. J. S. Lage, J. Stat. Phys. **64**, 653 (1991).

[2] W. S. Lo and R. A. Pelcovits, Phys. Rev. A **42**, 7471 (1990); M. Acharyya, Phys. Rev. E **56**, 1234 (1997); **56**, 2407 (1997); **58**, 179 (1998); **59**, 218 (1999); S. W. Sides, P. A. Rikvold, and M. A. Novotny, Phys. Rev. Lett. **81**, 834 (1998); Phys. Rev. E **59**, 2710 (1999); P. A. Rikvold *et al.*, in *Computer Simulation Studies in Condensed Matter Physics XIII*, edited by D. P. Landau, S. P. Lewis, and H.-B. Schüttler (Springer, Berlin, 2000), pp. 105–119; G. Korniss, C. J. White, P. A. Rikvold, and M. A. Novotny, Phys. Rev. E **63**, 016120 (2000).

[3] D. T. Robb, P. A. Rikvold, A. Berger, and M. A. Novotny, Phys. Rev. E **76**, 021124 (2007).

[4] Q. Jiang, H.-N. Yang, and G.-C. Wang, Phys. Rev. B **52**, 14911 (1995); J. Appl. Phys. **79**, 5122 (1996).

[5] H. Fujisaka, H. Tutu, and P. A. Rikvold, Phys. Rev. E **63**, 036109 (2001).

[6] T. Yasui, H. Tutu, M. Yamamoto, and H. Fujisaka, Phys. Rev. E **66**, 036123 (2002).

[7] N. Fujiwara, H. Tutu, and H. Fujisaka, Phys. Rev. E **70**, 066132 (2004); Prog. Theor. Phys. Suppl. **161**, 181 (2006); N. Fujiwara, T. Kobayashi, and H. Fujisaka, Phys. Rev. E **75**,

026202 (2007).
[8] J. Hausmann and P. Ruján, Phys. Rev. Lett. **79**, 3339 (1997); J. Phys. A **32**, 61 (1999); **32**, 75 (1999).
[9] M. Acharyya, Phys. Rev. E **58**, 174 (1998).
[10] W. Horsthemke and R. Lefever, *Noise-Induced Transitions* (Springer, Berlin, 1984).
[11] I. Bena, Int. J. Mod. Phys. B **20**, 2825 (2006).
[12] K. Ouchi, T. Horita, and H. Fujisaka, Phys. Rev. E **74**, 031106 (2006).
[13] K. Ouchi, N. Tsukamoto, H. Fujisaka, and T. Horita, J. Korean Phys. Soc. **50**, 201 (2007); K. Ouchi, N. Tsukamoto, T. Horita, and H. Fujisaka, Phys. Rev. E **76**, 041129 (2007).
[14] H. Fujisaka and T. Yamada, Prog. Theor. Phys. **74**, 918 (1985); **75**, 1087 (1986).
[15] T. Yamada and H. Fujisaka, Prog. Theor. Phys. **76**, 582 (1986); J. F. Heagy, N. Platt, and S. M. Hammel, Phys. Rev. E **49**, 1140 (1994); M. Ding and W. Yang, *ibid.* **52**, 207 (1995).
[16] T. John, U. Behn, and R. Stannarius, Phys. Rev. E **65**, 046229 (2002).
[17] N. Platt, E. A. Spiegel, and C. Tresser, Phys. Rev. Lett. **70**, 279 (1993); J. F. Heagy, N. Platt, and S. M. Hammel, Phys. Rev. E **49**, 1140 (1994).
[18] W. Feller, *An Introduction to Probability Theory and Its Applications*, 2nd ed. (Wiley, New York, 1971), Vol. 2, Chap. 13.
[19] H. Fujisaka and T. Yamada, Prog. Theor. Phys. **90**, 529 (1993).
[20] S. Miyazaki and H. Hata, Phys. Rev. E **58**, 7172 (1998).
[21] S. Miyazaki, T. Harada, and A. Budiyono, Prog. Theor. Phys. **106**, 1051 (2001); S. Miyazaki, T. Harada, K. Ito, and A. Budiyono, *Recent Ressearch Developments in Physics* (Kerala, India, 2003), Vol. 4, Part 1 pp. 155–190.
[22] V. Balakrishnan and S. Chaturvedi, Physica A **148**, 581 (1988).